

<https://doi.org/10.15407/ujpe70.4.271>

A.M. GUSAK,^{1,2} S.O. ABAKUMOV¹

¹ The Bohdan Khmelnytsky National University of Cherkasy
(81, Shevchenko Boul., Cherkasy 18031, Ukraine;
e-mails: amgusak@ukr.net, abakumov.serhii.official@gmail.com)

² Ensemble3 Centre of Excellence
(133 Wólczyńska Str., 01-919 Warsaw, Poland)

SIMPLIFIED KINETIC MODEL OF FLUX-DRIVEN PHASE TRANSITIONS AND PATTERNS COMPETITION IN OPEN 2D SYSTEM

The regular solution approximation has a successful history of applications in the thermodynamics and kinetics of decomposition in alloys, treated as closed systems. It provides a qualitatively proper description of all stages of spinodal and nucleation-mediated decomposition for alloys under homogeneous external conditions without external fluxes. In this article, the kinetic mean-field model for open (flux-driven) systems is extended by incorporating the divergence of in- and out-fluxes into the master equations for occupation probabilities. The closest experimental analog of this model is the pattern formation during the co-deposition of a binary alloy under frozen bulk diffusion, but with reasonable surface diffusion, where the deposition rate V serves as the main external parameter. However, some peculiarities of the model may also be useful for describing eutectic and off-eutectic crystallizations. Rate-dependent phase $T - C$ diagrams are determined for the steady states of such an open system. The rate-dependent instability region is subdivided into three distinct steady-state morphologies: spots (“gepard”-like), layers (“zebra”-like) – labyrinth or lamellae, and mixed patterns (a combination of “gepard” and “zebra”). This morphology map depends on the initial conditions, revealing memory effects and hysteresis. This implies that, unlike the equilibrium state of a closed system, which acts as an attractor for the evolution paths, the steady states of flux-driven systems may not be attractors. Variations of the model, including Monte Carlo simulations, are also discussed.

Keywords: open system, flux-driven transformation, spinodal decomposition, pattern formation, rate-dependent phase diagram, hysteresis.

1. Introduction

To begin, let us define the terms “closed” and “open” systems as used in this work. A thermodynamic system is referred to as “closed,” when it is subject to homogeneous external conditions across its boundaries. This typically includes cases such as:

- a) an isolated system,
- b) a system with a fixed volume within a thermal bath at a uniform temperature T ,

c) a system under a fixed homogeneous pressure within a thermal bath at a uniform temperature T .

In case (a), the system evolves toward the state of maximum entropy; in case (b), toward the minimum Helmholtz free energy, $F = U - TS$; and, in case (c), toward the minimum Gibbs free energy, $G = U - TS + pV$. By contrast, a system is described as “open,” if it experiences inflow and outflow of matter and/or energy, typically driven by gradients in the electrochemical potential, temperature, or stress. Such gradients cannot vanish over time due to boundary conditions, such as hot and cold ends of a system or opposite poles in an electrical circuit. While closed systems always progress toward an equilibrium, open systems may reach a steady state, exhibit oscillatory behavior, or even fail, but they do not reach the equilibrium. Thermodynamics, phase

Citation: Gusak A.M., Abakumov S.O. Simplified kinetic model of flux-driven phase transitions and patterns competition in open 2D system. *Ukr. J. Phys.* **70**, No. 4, 271 (2025). <https://doi.org/10.15407/ujpe70.4.271>.

© Publisher PH “Akademperiodyka” of the NAS of Ukraine, 2025. This is an open access article under the CC BY-NC-ND license (<https://creativecommons.org/licenses/by-nc-nd/4.0/>)

transitions, driving forces, partition functions, probability distributions, and the final equilibrium states of closed systems are well understood, although the principles governing the choice of evolutionary paths among multiple possibilities remain an open question. Many general behaviors of closed systems can be effectively studied using simple, fundamental models, such as the Ising model. In contrast, open systems remain far less understood, despite intensive analysis, particularly of non-equilibrium phase transitions [1].

An interesting approach was proposed by Martin, Bellon *et al.* for the modeling of open crystalline systems under irradiation or severe plastic deformation (SPD) [2–4]. Martin *et al.* refer to such situations as “driven systems” and introduce the concepts of ballistic jumps and effective temperature for their description. Their approach is built on well-known master equations for site occupancy probabilities, which change over time due to atomic exchanges (jumps). They consider two types of jumps: thermal (the usual transition probability of overcoming a barrier due to thermal fluctuations) and ballistic (athermal, depending on external energetic influences rather than temperature):

$$\frac{\partial P_i}{\partial t} = \sum_j (-P_i W_{i;j} + P_j W_{j;i}), \quad (1)$$

$$W_{j;i} = W_{j;i}^{\text{th}} + W_{j;i}^{\text{bal}}.$$

Our simplified model of open systems does not use the concept of ballistic jumps, but, instead it, adopts the idea of incoming atoms replacing existing ones randomly at the free surface due to an external flux, thereby “gradually transforming” surface atoms into bulk atoms with zero mobility. To better understand the general behaviors of open systems, we propose a model as elementary as the Ising model. The Ising model serves as a classic example for illustrating essential thermodynamic and kinetic features of phase transitions in closed systems [5]. In this work, we introduce an “Ising-like” model that maintains similar simplifications to study the principal features of open systems, particularly their steady states. For this purpose, we adopt Georges Martin’s modified approach, based on master equations for site occupancy probabilities. Martin first proposed a self-consistent nonlinear kinetic model for a quasi-1D system in 1990, [6] later applied to thin-film nonlinear interdiffusion across contact zones with pronounced diffusion asymmetry, typically confined to a few atomic layers (Erde-

lyi, Beke *et al.* [7, 8]). Subsequently, we developed a 3D model, [9–12] which has since formed the basis for a new software, SKMF (Stochastic Kinetic Mean-Field, skmf.eu), for atomistic simulations of diffusion-controlled transformations, including spinodal decomposition, nucleation, ripening, reactive diffusion, and phase competition. Recently, we applied the 2D version of SKMF to examine the pattern formation during the vapor co-deposition of binary alloys [13]. Pattern formation on the mesoscopic scale during the crystallization from liquid or vapor phases is well-studied [14–19], yet the atomic-scale pattern formation remains relatively underexplored [20]. In our previous work, [13] we used a somewhat artificial model, assuming that a new atomic (001) plane in the FCC lattice is rapidly filled by incoming atoms. Afterward, atomic exchanges occur over a time $\frac{\delta}{V}$ where V is the deposition velocity, equal to the product of deposition flux density and the atomic volume of the solid phase, and δ is the interplanar spacing in the deposition direction). Following this period, diffusion within the “buried” atomic plane is considered fully frozen.

2. Basic Model Assumptions

In this version of our model, we aim to create a time-continuous framework that avoids stepwise kinetics involving abrupt avalanches of atomic plane filling followed by isolated diffusion within the plane. Instead, we introduce a “smeared” timescale in which diffusion within the top surface layer and deposition occur simultaneously. This approach allows us to use a moving reference frame that travels with the top surface at a constant velocity V in the deposition direction. In this moving frame, in addition to diffusion fluxes along the plane (leading to partial decomposition), there are two external fluxes perpendicular to the top surface: an inflow $\frac{V}{\Omega} C^{\text{dep}}$ (where Ω is the atomic volume in the solid phase) and an outflow $\frac{V}{\Omega} C_A(i, j, k = 0)$, with $k = 0$ indicating the top plane and i, j denoting specific lattice sites within it (in an FCC lattice, $i + j + k$ is even). Both processes – the diffusion along the top plane and the flux divergence across it – are mathematically represented by two terms on the right-hand side of Eq. (2), which governs the site occupancy probabilities:

$$\frac{\partial C_A}{\partial t} = \sum_{i=1}^{Z_{\parallel}} \left\{ -C_A(i) C_B(in) \Gamma_{AB} (A(i) \leftrightarrow B(in)) + \right.$$

$$+ C_B(i) C_A(in) \Gamma_{AB} \left(A(in) \leftrightarrow B(i) \right) \Big\} + \frac{V}{\delta} (C^{\text{dep}} - C_A(i)). \quad (2)$$

Analogic modification of diffusion equation for the linear version of Cahn–Hilliard approach was discussed in [21].

Here, $C_A(i)$ actually represents $C_A(i, j, k = 0)$ and is the probability of site (i, j) ($x = \frac{a}{2}i$, $y = \frac{a}{2}j$) in the top plane ($k = 0$) ($z = \frac{a}{2}0$) being occupied by species A . We consider only an FCC monocrystalline lattice grown by the deposition in the $\langle 001 \rangle$ direction, where $i + j + k$ is an even number. In our model, atomic exchanges occur only between sites within the same top plane ($k_n = 0$, $i_n + j_n + k_n = \text{even}$). Exchange frequencies are determined by a Boltzmann-like expression:

$$\Gamma_{AB} (A(i) \leftrightarrow B(in)) = \nu_0 \exp \left[- \frac{E^s - (E_A(i) + E_B(in))}{kT} \right], \quad (3)$$

where $(E_A(i) + E_B(in)) = (E_A(i, j, k = 0) + E_B(in, j_n, k_n = 0))$ is the interaction energy of neighboring atoms before the exchange, and E^s is the saddle-point energy during the exchange (assumed constant in the original Martin model and all its developments).

Energies are calculated in a mean-field approximation and include $Z_{\parallel} = 4$ nearest neighbors from the same top plane ($k = 0$) with indexes $(i \pm 1, j)$ and $(i, j \pm 1)$, as well as $Z_{\perp} = 4$ nearest neighbors from the plane below ($k = 1$, $z = -\frac{a}{2}1$) with indices $(i \pm 1, j)$ and $(i, j \pm 1)$

$$E_A(i) = \sum_{i'=1}^{Z_{\parallel}+Z_{\perp}} \left\{ C_A(i') V_{AA} + C_B(i') V_{AB} \right\} = (Z_{\parallel} + Z_{\perp}) V_{AB} + (V_{AA} - V_{AB}) \sum_{i'=1}^{Z_{\parallel}+Z_{\perp}} C_A(i'), \quad (4)$$

$$E_B(in) = \sum_{in'=1}^{Z_{\parallel}+Z_{\perp}} \left\{ C_A(in') V_{BA} + C_B(in') V_{BB} \right\} = (Z_{\parallel} + Z_{\perp}) V_{BB} + (V_{AB} - V_{AA}) \sum_{in'=1}^{Z_{\parallel}+Z_{\perp}} C_A(in'). \quad (5)$$

For co-deposition of $\langle 001 \rangle$ planes of an FCC lattice, the number of nearest neighbors within the top plane (simultaneously the number of possible atomic exchanges) is $Z_{\parallel} = 4$, while the number of nearest neighbors in the preceding (subsurface) plane is $Z_{\perp} = 4$. “ i ” and “ in ” are two neighboring sites within the top atomic plane, exchanging atoms. At a fixed “ i ,” there are $Z_{\parallel} = 4$ possibilities for “ in ”. “ i ” represents the nearest interacting neighbors of site “ i ,” and their number is $Z = Z_{\parallel} + Z_{\perp} = 8$, similarly, “ in ” represents the nearest interacting neighbors of site “ in ,” and their number is also $Z = Z_{\parallel} + Z_{\perp} = 8$.

To simplify calculations, we postulate that the probabilities in the subsurface plane $k = 1$ are entirely determined by their nearest neighbors in the top plane $k = 0$:

$$C_A(i, j, k = 1) = \frac{1}{4} \left[C_A(i + 1, j, k = 0) + C_A(i - 1, j, k = 0) + C_A(i, j + 1, k = 0) + C_A(i, j - 1, k = 0) \right]. \quad (6)$$

This assumption, while not absolute, works well for decomposition, as demonstrated later.

For simplicity, we also assume: $V_{AA} = 0$, $V_{BB} = 0$, $V_{AB} = E_{\text{mix}}$. Thus:

$$\Gamma_{AB} (A(i) \leftrightarrow B(in)) = \nu_0 \exp \left[- \frac{E^s}{kT} \right] \times \exp \left[\frac{E_{\text{mix}}}{kT} \left(Z - \sum_{i'=1}^Z C_A(i') + \sum_{in'=1}^Z C_A(in') \right) \right], \quad (7)$$

$$\Gamma_{AB} (A(in) \leftrightarrow B(i)) = \nu_0 \exp \left[- \frac{E^s}{kT} \right] \times \exp \left[\frac{E_{\text{mix}}}{kT} \left(Z - \sum_{in'=1}^Z C_A(in') + \sum_{i'=1}^Z C_A(i') \right) \right]. \quad (8)$$

The master equation for site occupancy probabilities within the surface layer $k = 0$ becomes:

$$\frac{\partial C_A(i)}{\partial t} = \sum_{in=1}^{Z_{\parallel}} \left\{ -C_A(i)(1 - C_A(in)) \times \exp \left[\frac{E_{\text{mix}}}{kT} \left(\sum_{in'=1}^Z C_A(in') - \sum_{i'=1}^Z C_A(i') \right) \right] + (1 - C_A(i)) C_A(in) \times \exp \left[\frac{E_{\text{mix}}}{kT} \left(\sum_{i'=1}^Z C_A(i') - \sum_{in'=1}^Z C_A(in') \right) \right] \right\} + \nu (C^{\text{dep}} - C_A(i)), \quad (9)$$

where the non-dimensional time and velocity parameters are:

$$tt = t\nu_0 \exp\left[\frac{ZE_{\text{mix}} - E^s}{kT}\right], \quad (10)$$

$$v = \frac{V}{\delta\nu_0 \exp\left[\frac{ZE_{\text{mix}} - E^s}{kT}\right]}.$$

In this study, we focus on the case of positive mixing energy, which corresponds to a tendency toward decomposition. Depending on temperature, composition, and deposition velocity, decomposition may be realized partially or not at all.

3. Binodal and Spinodal in KMF Model at Zero Rate (Decomposition in a Closed System)

In this section, we verify whether our atomistic, non-linear KMF model adheres to the standard binodal and spinodal concepts for closed systems ($V = 0$).

3.1. Binodal (thermodynamic two-phase equilibrium which can be reformulated as detailed flux balance)

First, we consider the equilibrium condition at $V = 0$, which corresponds to the balance equations derived from Eq. (2):

$$C_A(i) (1 - C_A(in)) \Gamma_{AB}(A(i) \leftrightarrow B(in)) = (1 - C_A(i)) C_A(in) \Gamma_{AB}(A(in) \leftrightarrow B(i))$$

or

$$C_A(i) (1 - C_A(in)) \exp\left[-\frac{E^s - (E_A(i) + E_B(in))}{kT}\right] = (1 - C_A(i)) C_A(in) \exp\left[-\frac{E^s - (E_A(in) + E_B(i))}{kT}\right], \quad (11)$$

which can be reformulated as:

$$(E_A(i) + kT \ln C_A(i)) - (E_B(i) + kT \ln C_B(i)) = (E_A(in) + kT \ln C_A(in)) - (E_B(in) + kT \ln C_B(in)). \quad (12)$$

Since $E_A(i) + kT \ln C_A(i) = \mu_A(i)$ is a local chemical potential of A , and $E_B(i) + kT \ln C_B(i) = \mu_B(i)$ – that of B , their difference $\mu_{AB}(i) \equiv \mu_A(i) - \mu_B(i)$ is just a reduced chemical potential (change of Gibbs

free energy due to the replacement of atom B by atom A). Equality of the reduced chemical potential across different sites indicates thermodynamic equilibrium, including cases where these sites belong to distinct phases (e.g., solid solutions on opposite sides of the binodal). For such cases, $C_A(i) = C_A(i') = C_A(\alpha)$, $C_A(in) = C_A(in') = C_A(\beta) = 1 - C_A(\alpha)$. Substituting it into Eq. (9) under conditions $v = 0$, $\frac{\partial C_A(i)}{\partial tt} = 0$, after simple algebra, we get:

$$\frac{C_A(\alpha)}{1 - C_A(\alpha)} = \exp\left[-\frac{8E_{\text{mix}}}{kT} (1 - 2C_A(\alpha))\right]. \quad (13)$$

This expression matches the binodal equation for the regular solution model with eight nearest neighbors per site.

3.2. Instability criterion for a closed system (spinodal)

Typically, the concept of infinitesimal concentration waves, which may exponentially increase or decrease depending on the wave vector, temperature, and composition, is attributed to Cahn and Hilliard in their phenomenological analysis of the spinodal decomposition [22]. However, a similar idea for the instability criterion of non-linear kinetic equations was proposed much earlier for the atomic scale by Anatoliy Vlasov in his non-local statistical approach to crystals [23]. Later, analogous concepts were also applied on the atomic scale by Armen Khachatryan in his theory of concentration waves [24]. In our KMF model, we seek a solution in the form of an atomic-scale concentration wave with an infinitesimal time-dependent amplitude A :

$$C_A(i, j, k = 0) = C^{\text{dep}} + \delta C(i, j, k = 0) = C^{\text{dep}} + A(tt, \mathbf{q}) \exp[I\mathbf{q} \cdot \mathbf{r}_{i,j}] = C^{\text{dep}} + A(tt, q_x, q_y) \exp\left[I\frac{a}{2}(q_x i + q_y j)\right]. \quad (14)$$

Here, I is the imaginary unit, $\sqrt{-1}$. Then, according to our condition (Eq. (6)), for the sites of sublevel ($k = 1$), the concentration wave is:

$$C_A(i', j', k = 1) = \frac{1}{4} \left[C_A(i' + 1, j', k = 0) + C_A(i' - 1, j', k = 0) + C_A(i', j' + 1, k = 0) + C_A(i', j' - 1, k = 0) \right] =$$

$$\begin{aligned}
&= C^{\text{dep}} + A \exp\left[I\frac{a}{2}(q_x i' + q_y j')\right] \frac{1}{4} \left[\exp\left(I\frac{a}{2}q_x\right) + \right. \\
&+ \exp\left(-I\frac{a}{2}q_x\right) + \exp\left(I\frac{a}{2}q_y\right) + \exp\left(-I\frac{a}{2}q_y\right) \left. \right] = \\
&= C^{\text{dep}} + A \exp\left[I\frac{a}{2}(q_x i' + q_y j')\right] \times \\
&\times \frac{1}{2} \left[\cos\left(\frac{a}{2}q_x\right) + \cos\left(\frac{a}{2}q_y\right) \right]. \quad (15)
\end{aligned}$$

Substituting Eqs. (14) and (15) into Eq. (9), expanding everything into a series over small A and neglecting second-order and higher-order terms, a simple algebra (Appendix A) leads to the following stability/instability criterion for the amplitudes of concentration fluctuation waves:

$$\begin{aligned}
\frac{\partial \ln A}{\partial tt} &= 4 \left[1 - \cos\left(q_x \frac{a}{2}\right) \cos\left(q_y \frac{a}{2}\right) \right] \times \\
&\times \left\{ \frac{16E_{\text{mix}}}{kT} C^{\text{dep}} (1 - C^{\text{dep}}) f(q_x, q_y) - 1 \right\}, \quad (16)
\end{aligned}$$

$$\begin{aligned}
f(q_x, q_y) &= \frac{1}{2} \cos\left(q_x \frac{a}{2}\right) \cos\left(q_y \frac{a}{2}\right) + \\
&+ \frac{1}{8} \left(\cos\left(q_x \frac{a}{2}\right) + \cos\left(q_y \frac{a}{2}\right) \right)^2. \quad (17)
\end{aligned}$$

Instability case: $\frac{\partial \ln A}{\partial tt} > 0$. Taking into account that $f(q_x, q_y) \leq 1$, the condition of instability is $\frac{16E_{\text{mix}}}{kT} C^{\text{dep}} (1 - C^{\text{dep}}) > 1$, which coincides with the spinodal criterion in the regular solid solution model at $Z = 8$.

4. Rate-Dependent Binodal in Open System

Here, we discuss a binodal-like solution – a steady state instead of equilibrium. As follows from Eq. (7), in the case of open systems, the “binodal-like” condition includes an additional rate-dependent term:

$$\begin{aligned}
v(C_A(i) - C^{\text{dep}}) &= \sum_{in=1}^{Z_{\parallel}} \left\{ -C_A(i) (1 - C_A(in)) \times \right. \\
&\times \exp\left[\frac{E_{\text{mix}}}{kT} \left(\sum_{in'=1}^Z C_A(in') - \sum_{i'=1}^Z C_A(i') \right)\right] + \\
&+ (1 - C_A(i)) C_A(in) + \\
&+ \left. \exp\left[\frac{E_{\text{mix}}}{kT} \left(\sum_{i'=1}^Z C_A(i') - \sum_{in'=1}^Z C_A(in') \right)\right] \right\}. \quad (18)
\end{aligned}$$

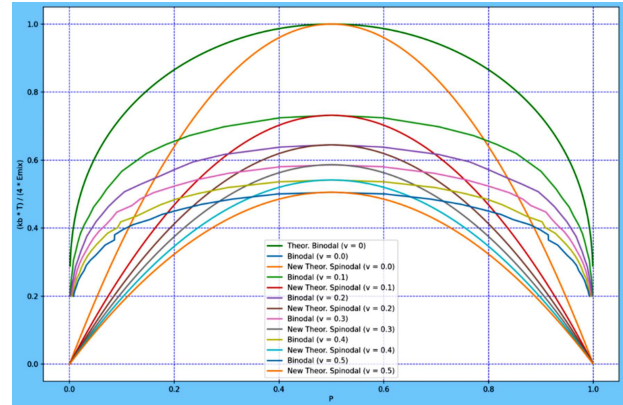


Fig. 1. Rate-dependent binodals and rate-dependent spinodals at $\nu = 0, 0.1, 0.2, 0.3, 0.4, 0.5, \dots$. Binodals are found from the averaging of marginal compositions

So far, we cannot suggest a natural interpretation of this condition, as we did with the detailed balance and equality of reduced chemical potentials for the closed system in Eqs. (11) and (12). Thus, we numerically simulated decomposition by solving the set of Eqs. (9) and tracking the solution until it practically satisfied Eq. (18). In that process, we fixed the maximal (right part of the binodal) and minimal (left part of the binodal) concentrations within our system, allowing for small corrections due to noise and Gibbs–Thomson corrections at the curved interfaces. Of course, the tendency toward the steady state of the solution to Eq. (9) should lead to the validity of Eq. (18), at least in the case where initial inhomogeneities are large enough to overcome the nucleation barrier of decomposition. The result – rate-dependent binodals (as well as rate-dependent spinodals in Section 5) – is shown in Fig. 1. We emphasize an important difference between the binodal in closed and open systems: In a closed system, any point below the binodal corresponds to an alloy that will decompose – via the spinodal decomposition of an absolutely unstable solution, if this point is simultaneously below the spinodal, or via a “nucleation-growth-ripening” process in the metastable solution, if this point is between the binodal and spinodal. In both cases, the result is the same: the system transforms into a two-phase state with two marginal compositions corresponding to the binodal. In an open system, as we will see in Section 7, the situation is ambiguous in several aspects:

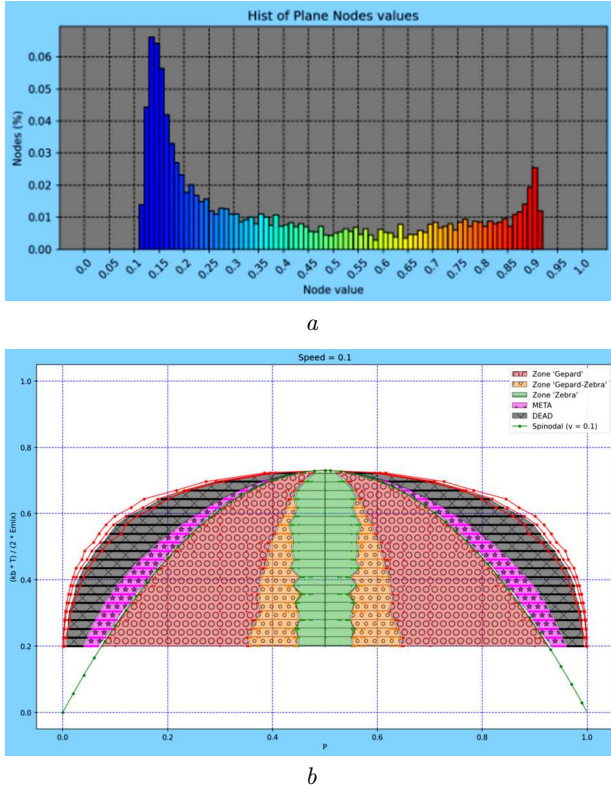


Fig. 2. Smearred (splitted) binodal for steady-states in an open system. Histogram of compositions in the decomposed steady-state of the open system, $C = 0.4$ (a); Binodal as a bunch of curves-only marginal curves and the mean curve are shown, the regions within the binodal will be described below. In all Figures below, we will use only the mean binodal (b)

1) If the composition of the incoming flux belongs to the spinodal region and is equal to the initial composition, it decomposes and finally reaches a steady-state two-phase morphology, which is not equilibrium and not uniform within each phase, since, in steady-state, the divergence of in- and out-fluxes should be compensated by the divergence of lateral redistribution fluxes. This means that, in steady state, contrary to the equilibrium decomposed state in a closed system, the system does not demonstrate the two distinct compositions of the binodal curve, but rather the whole composition spectrum. An example of such a composition histogram in the steady state is shown in Fig. 2, a. One may roughly interpret the compositions corresponding to the minimum and maximum of this histogram as a “smearred”binodal – typically, these marginal compositions are quite close to the two peaks of the mentioned histogram.

276

2) Typically, marginal compositions are close but different for two different alloys with different compositions of the incoming flux. It means that, strictly speaking, for an open system, the rate-dependent binodal is not a curve, but rather something like a “smearred” curve, or, in other words, a “bunch” of binodals. An example of such a bunch is shown in Fig. 2, b.

3) If the composition of the incoming flux belongs to the interdome region (beyond the spinodal, but within the binodal), it, indeed, leads to the decomposition (if pre-existing structures are used as the initial condition), while another part shows a full absence of decomposition. In this sense, the rate-dependent binodal is “smearred”, like the size-dependent binodal for nanoparticles [25–27].

5. Rate-Dependent Spinodal – Instability in Respect to Infinitesimal Perturbations

In full analogy with subsection 3.2, for the open system, the criterion for absolute instability and subsequent decomposition is reduced to the positive sign of the following derivative:

$$\frac{\partial \ln A}{\partial t} = -v + 4 \left[1 - \cos\left(q_x \frac{a}{2}\right) \cos\left(q_y \frac{a}{2}\right) \right] \times \left\{ \frac{8E_{\text{mix}}}{kT} C^{\text{dep}} (1 - C^{\text{dep}}) f(q_x, q_y) - 1 \right\}, \quad (19)$$

(where f is determined by Eq. (17))

This means that, at a fixed composition of the deposition flux and a fixed temperature, the alloy can be stabilized against the decomposition by the velocity:

$$v > v^{\text{critical}} = \max(\text{in respect to } q_x, q_y) \times \left\{ 4 \left[1 - \cos\left(q_x \frac{a}{2}\right) \cos\left(q_y \frac{a}{2}\right) \right] \times \left[\frac{8E_{\text{mix}}}{kT} C^{\text{dep}} (1 - C^{\text{dep}}) f(q_x, q_y) - 1 \right] \right\}. \quad (20)$$

In Appendix B, we show that the maximum is reached for concentration waves along the diagonal direction $\langle 110 \rangle$, $\mathbf{q} = \left(\frac{q}{\sqrt{2}}, \frac{q}{\sqrt{2}}, 0\right)$, $\cos^2\left(\frac{qa}{2\sqrt{2}}\right) = \frac{W+1}{2W}$, (here $W = \frac{16E_{\text{mix}}}{kT} C^{\text{dep}} (1 - C^{\text{dep}}) > 1$).

Thus, the critical velocity is:

$$v^{\text{critical}}(\langle 110 \rangle) = \frac{(W-1)^2}{W}. \quad (21)$$

From Eq. (21), we obtain the velocity-dependent spinodal curve for the open system:

$$\frac{kT}{4E_{\text{mix}}} = \frac{4C(1-C)}{1 + \frac{v}{2} + \sqrt{\left(1 + \frac{v}{2}\right)^2 - 1}}. \quad (22)$$

6. Morphology Maps for Steady-State (Amplitude of Initial Noise 0.001, Dynamic Zoise Zero)

If we use a homogeneous alloy with small initial fluctuations in the composition (e.g., 0.01), the decomposition in a steady-state occurs only for concentrations and temperatures under the rate-dependent spinodals. These regions are divided into three types of final steady morphologies: Gepard (spots), mixed morphology Gepard + Zebra, and Zebra (layered morphology – labyrinth or lamellae) – see Figs. 3 and 4.

7. Influence of Pre-Existing Structures: Decomposition Beyond Rate-Dependent Spinodal (as a Result of Composition or Temperature Shift from the Spinodal Region)

In closed systems, any alloy between the spinodal and binodal demonstrates decomposition via the nucleation-precipitation-coarsening mechanism. Since waiting for nucleation can take a very long time, one may use pre-existing structures to initiate the decomposition. In the case of an open system, to accelerate the process, we use the structures formed at a previous composition or temperature. By this method, we were able to reach steady-state decomposition only within a part of the region between the binodal and spinodal, attaching to the spinodal – see Fig. 5.

8. Hysteresis

As we can see from above, our model system exhibits some memory of the final state with respect to the initial conditions. This means that one can expect the hysteresis effect, when each new morphology is obtained in the system using the previous morphology as the initial condition. In this case, we can shift, step by step, the initial concentration (first from right to left, and then in the reverse direction – subsection 8.1), or we can shift, step by step, the temper-

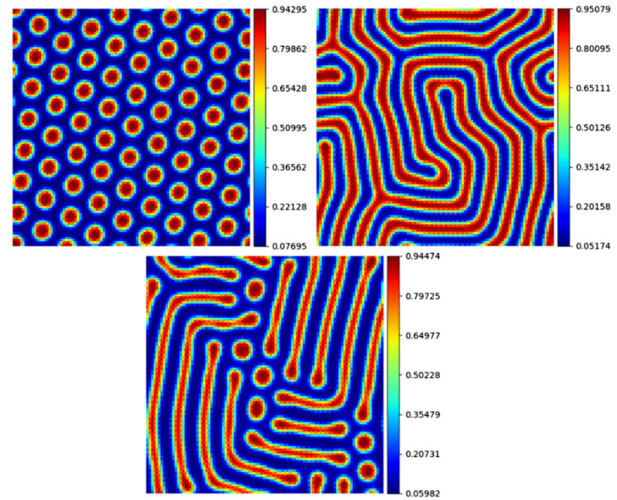


Fig. 3. Three main types of morphology in the case of decomposed steady-state: Gepard (spots), and Zebra (layered morphology – labyrinth or lamellae), mixed morphology Gepard + Zebra

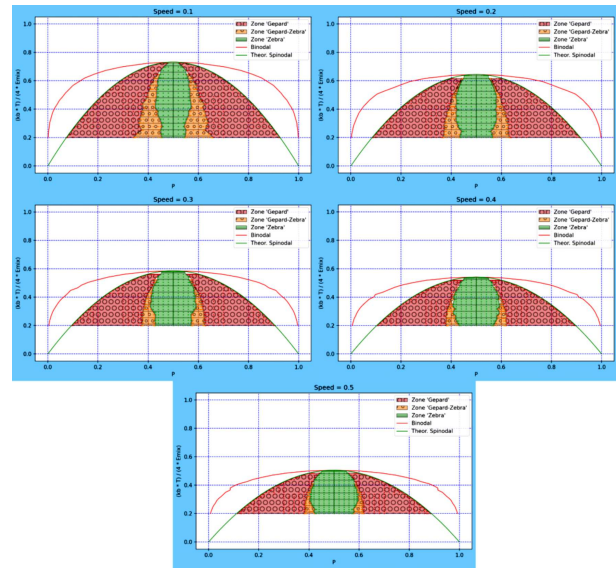


Fig. 4. Map of steady-state morphologies, obtained with the initial condition of a homogeneous alloy with small noise amplitude under rates $v = 0, 0.1, 0.2, 0.3, 0.4, 0.5, \dots$. Here we choose the mean value from the bunch of binodals

ature (first from low to high, and then from high to low – subsection 8.2).

8.1. Compositional hysteresis

First, we obtain the steady-state pattern for composition $C = 0.50$, simulated from homogeneous ini-

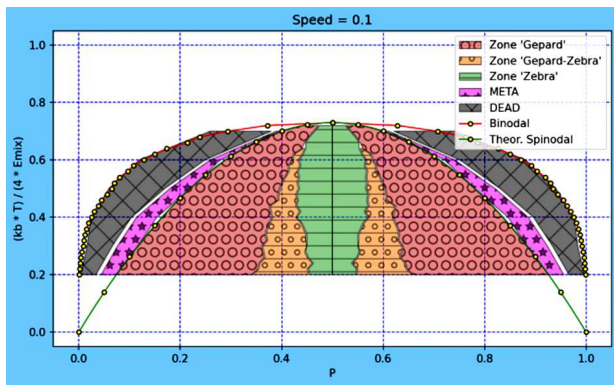


Fig. 5. Violet regions beyond the spinodal demonstrating the formation of steady-state gepard-like morphology on the basis of pre-existing structures. Case $v = 0.1$

tial conditions with a small initial noise amplitude of 0.001 at a constant temperature $kT/E_{\text{mix}} = 2$. We use this as the initial condition for the sample with $C = 0.49$, and so on, until $C = 0.20$. Then we start to move back upward in concentration, finishing with $C = 0.50$. In Fig. 6, we compare the steady-state morphologies for $C = 0.50$, obtained (first) from homogeneous initial conditions, and (second) as the last step of the step-by-step increase in C starting from 0.20. Two morphologies for $C = 0.49$ are obtained from $C = 0.50$ (and down) and from $C = 0.48$ (and up), and so on. We observe a significant hysteresis with respect to the direction of the concentration shift: Going down from 0.50 preserves the Zebra morphology until $C = 0.38$, while going up preserves the Gepard morphology up to $C = 0.47$.

8.2. Temperature hysteresis

We used a constant concentration $C = 0.30$ and changed the temperature kT/E_{mix} from 0.8 to 2.4 and then back down. We can observe that the type of morphology remains almost the same (if we ignore faceting), but the mean size and interparticle distances differ (Fig. 7).

9. Evolution Criterion

For a closed system in a thermal bath at fixed temperature and volume, the evolution criterion should coincide with the second law of thermodynamics' the time derivative of the Helmholtz free energy should be negative and tend to zero, indicating an equilibrium state with minimal free energy. Let us examine the behav-

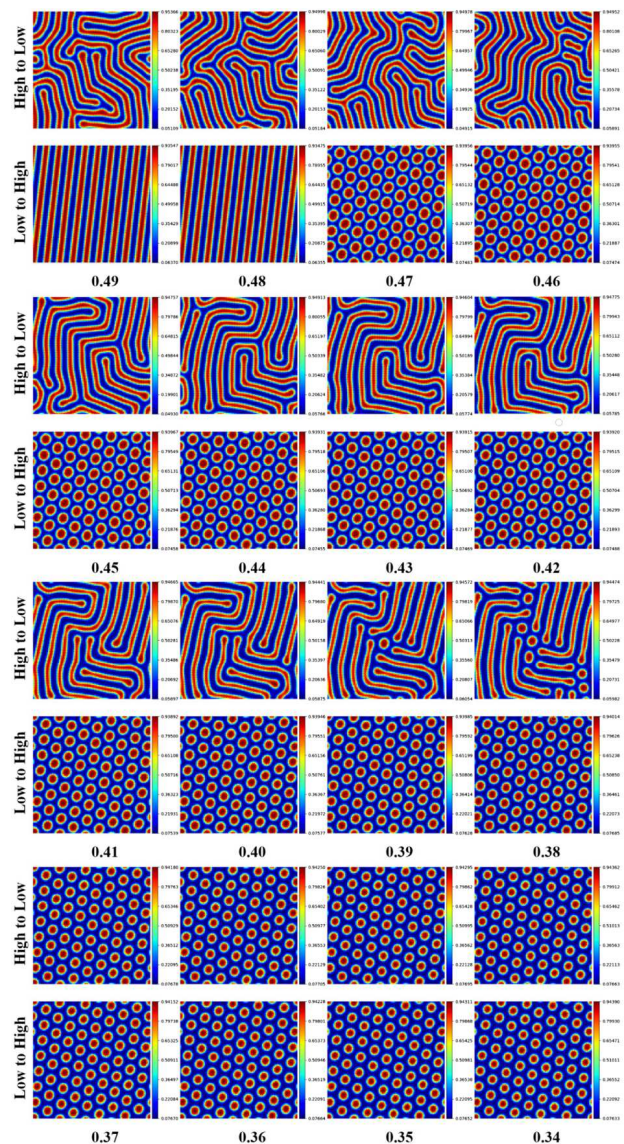


Fig. 6. Comparison of steady-state morphologies for the same composition, obtained from the pre-existing structures with higher and lower concentrations of A as the initial condition

ior of free energy in our simplified model system (and check, if it reduces to the minimization of the free energy in the case of zero rate). In the general case, the change rate of the free energy should consist of the following terms: (1) in-flux of free energy corresponding to the homogeneous solid solution $\frac{V}{\delta} F \{C^{\text{dep}}\}$ in all sites, (2) out-flux of free energy with the actual redistributed concentration $-\frac{V}{\delta} F \{C(\mathbf{r})\}$, (3) change rate due to atomic exchanges within the system

$[dF/dt]_{\text{inner}} = \sum_{(i,in)}^{NZ_{\parallel}/2} (\mu_{AB}(i) - \mu_{AB}(in)) \frac{dC^{i,in}}{dt}$, where $\frac{dC^{i,in}}{dt}$ is a partial change rate of site “ i ” occupancy by A (and simultaneously the partial change rate of site “ in ” occupancy by B due to exchange only between these two sites:

$$\frac{dC^{i,in}}{dt} = -C_A(i) C_B(in) \Gamma_{AB}(A(i) \leftrightarrow B(in)) + C_B(i) C_A(in) \Gamma_{AB}(A(in) \leftrightarrow B(i)).$$

As shown in Ref. [8], $[dF/dt]_{\text{inner}}$ can be reorganized to the form:

$$\begin{aligned} [dF/dt]_{\text{inner}} &= -\nu_0 \exp\left[-\frac{E^s}{kT}\right] \times \\ &\times \sum_{(i,in)}^{NZ_{\parallel}/2} (\mu_{AB}(i) - \mu_{AB}(in)) \left\{ \exp\left[\frac{\mu_{AB}(i)}{kT}\right] - \right. \\ &- \exp\left[\frac{\mu_{AB}(in)}{kT}\right] \left. \right\} \times C_B(i) C_B(in) \times \\ &\times \exp\left[\frac{E_B(i) + E_B(in)}{kT}\right], \end{aligned}$$

which is similar to the expression in Boltzmann derivation of the H-theorem and is always negative. Thus:

$$\begin{aligned} \frac{dF}{dt} &= \frac{V}{\delta} [F\{C^{\text{dep}}\} - F] + [dF/dt]_{\text{inner}}, \\ [dF/dt]_{\text{inner}} &\leq 0 \end{aligned}$$

for a closed system at fixed T . This property can be reformulated as

$$\left\{ \exp\left[-\frac{V}{\delta}t\right] \frac{d}{dt} \exp\left[\frac{V}{\delta}t\right] \right\} (F - F\{C^{\text{dep}}\}) \leq 0. \quad (23)$$

Equation (23) is a generalized evolution criterion for our model of the open system.

10. Possible Modification of the Model – Single Plane Instead of Two Planes ($Z_{\parallel} = 4, Z_{\perp} = 0$)

The model can be simplified further, if one considers not only exchanges, but also interactions within a single top plane. Elementary derivations (similar to Appendices A and B) lead to the following equations for the critical non-dimensional velocity and the rate-dependent spinodal:

$$v^{\text{critical}}(\text{single top plane}) = \frac{(W-2)^2}{2W}, \quad (24)$$

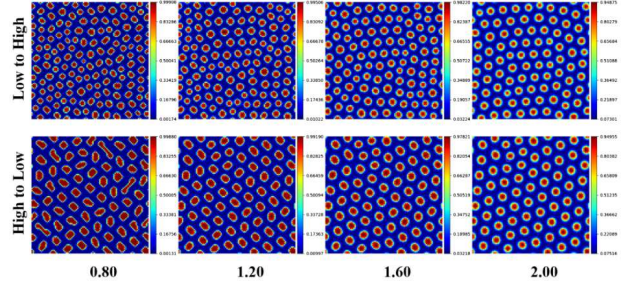


Fig. 7. Comparison of steady-state morphologies for the same temperature, obtained from the pre-existing structures for higher and lower temperatures as the initial condition

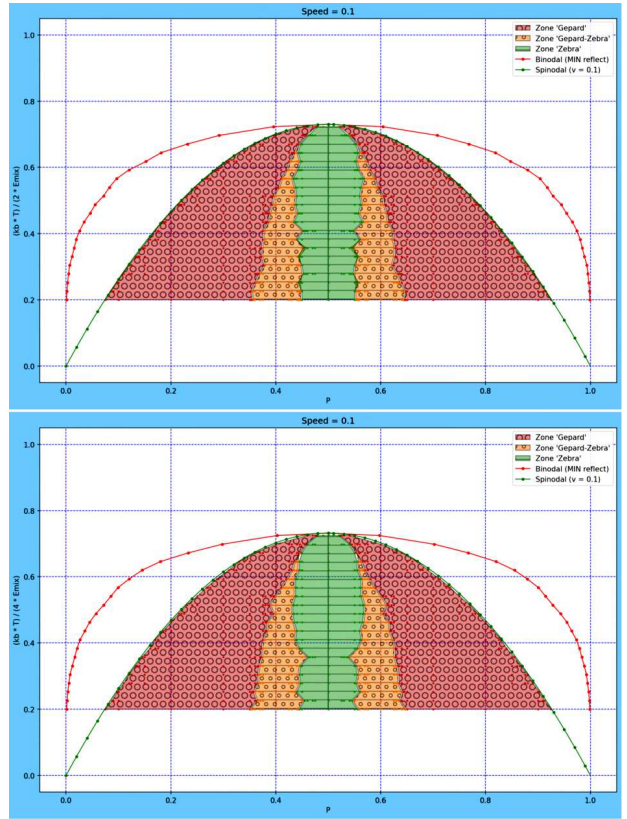


Fig. 8. Comparison of morphology map for models with two planes and single plane. One may see that after rescaling to non-dimensional temperature T/T_{crit} the maps practically coincide

$$\left(\frac{kT}{2E_{\text{mix}}}\right)_{\text{single top plane}} = \frac{4C(1-C)}{1 + \frac{v}{2} + \sqrt{\left(1 + \frac{v}{2}\right)^2 - 1}}. \quad (25)$$

Figure 8 shows a comparison of the mapping of patterns as a function of temperature and deposition rate

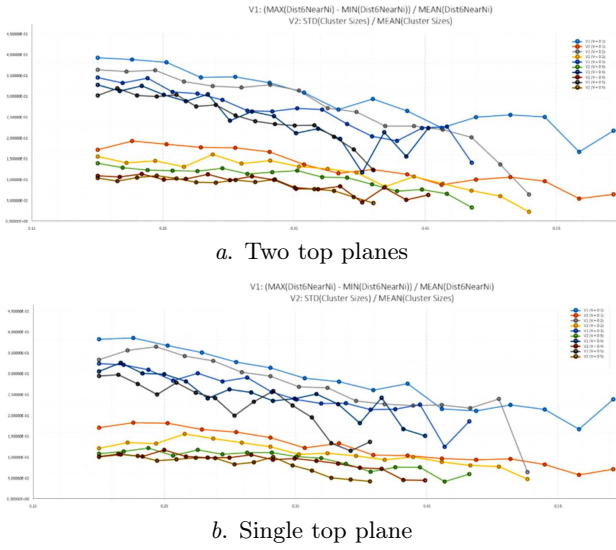


Fig. 9. Ratio V_1 of the scatter of distances to mean distance among nearest 6 neighbors, and ratio V_2 of the scatter of cluster sizes to the mean size, as the functions of reduced temperature ($kT/4E_{\text{mix}}$ for case (a) and $kT/2E_{\text{mix}}$ for case (b)) at various reduced rates v from 0.1 to 0.5. Composition of the incoming flux is $C = 0.3$ in all cases here

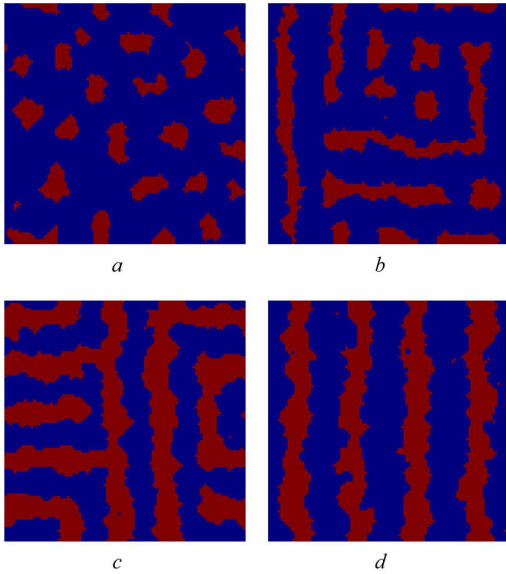


Fig. 10. Typical morphologies, obtained for single-plane model by Monte-Carlo method. Spots (Gepard), $C_{\text{dep}} = 0.2$, $v = 0.1$ ($P_{\text{dep}} = 0.000083$), $kT/E_{\text{mix}} = 0.4$ (a); Mixed (Gepard + Zebra), $C_{\text{dep}} = 0.3$, $v = 0.1$ ($P_{\text{dep}} = 0.000083$), $kT/E_{\text{mix}} = 0.4$ (b); Layers - labyrinth (Zebra1), $C_{\text{dep}} = 0.5$, $v = 0.1$ ($P_{\text{dep}} = 0.000083$), $kT/E_{\text{mix}} = 0.452$ (c); Layers - lamellae (Zebra2), $C_{\text{dep}} = 0.4$, $v = 0.1$ ($P_{\text{dep}} = 0.000083$), $kT/E_{\text{mix}} = 0.557$ (d)

for the main model with two planes and the model with a single top plane. One can see that after rescaling the temperature by a factor of 2, the maps practically coincide.

11. Ordering of Patterns with Change of Rate and Temperature

With increasing rate (velocity) v and temperature kT/E_{mix} the patterns have a tendency of ordering – distribution of distances between nearest neighbors and distribution of sizes become more narrow. We checked it for gepard-like morphology in both models – initial one (with exchanges within single plane but interactions in two planes), and in simplified model (both exchanges and interactions within single plane). First, we calculated the distances from the cluster centers to the centers of 6 nearest neighbors for each spot, then found the difference of maximal and minimal distances among these six, then calculated the ratio of this difference and average distance, and then took average over all spots. Second, we calculated the sizes (number of atoms) of each cluster, then found the deviation of size over all spots, and then calculated the ratio of deviation and mean size. The typical results are shown in Fig. 9 for initial model (a) and for simplified model (b).

12. Monte-Carlo Version of the Model

So far, all simulations were conducted within the framework of the non-linear mean-field self-consistent atomic approximation KMF (Kinetic Mean-Field). To build the Monte Carlo version of our simplified model, which includes interactions within a single top plane, we start with the standard Metropolis algorithm for the exchange mechanism in a 2D lattice, but add the probability P_{dep} of replacing any atom with a new atom of type A with probability C^{dep} and type B with probability $1 - C^{\text{dep}}$. The probability P_{dep} is proportional to the non-dimensional deposition rate: $P_{\text{dep}} = \alpha v$. To find the proportionality factor α , we calculated the critical temperature (top of the rate-dependent spinodal) from Eq. (25):

$$\frac{kT_{\text{crit}}}{2E_{\text{mix}}} = \frac{1}{1 + \frac{v}{2} + \sqrt{(1 + \frac{v}{2})^2 - 1}}$$

for $v = 0.1$ – it was 0.642, and then in Monte Carlo scheme, for this temperature and for $C^{\text{dep}} = 0.5$, found at which probability P_{dep} we get the margin

of stability (larger P_{dep} – stable alloy, smaller P_{dep} – decomposition starts). Such fitting gave us

$$\alpha = 0.00083. \quad (26)$$

Typical morphologies, obtained by Monte Carlo at various composition of incoming flux, at the same velocity but varying temperatures, are shown in Fig. 10.

13. Conclusions

1. We developed a model of a 2D regular solid solution for an open system, characterized by an additional rate parameter – the deposition rate, V . For non-zero constant V , this model system reaches a steady state, rather than equilibrium.

2. We analytically derived and numerically validated the rate-dependent spinodal for alloys that are entirely unstable with respect to any fluctuation. Increasing V stabilizes the alloy, lowering the spinodal curve, as shown in Eqs. (20) and (21).

3. If the initial system composition is nearly uniform with minor fluctuations, and the deposited composition-temperature point lies below the rate-dependent spinodal, the resulting state stabilizes into one of two primary morphologies (Figs. 3 and 4): “cheetah”(gепard-like, spot-like) or “zebra” (layered, in the form of labyrinths or parallel lamellae). In a narrow transition zone, a mixture of these two morphologies emerges.

4. The rate-dependent binodal has been determined only numerically, by directly measuring the marginal compositions in the asymptotic steady states (Fig. 1). The “interdome region” in the phase diagram (points beyond the spinodal, but within the binodal) is subdivided into two subregions – see the next conclusion.

5. In the before-mentioned intermediate regions between the rate-dependent binodals and rate-dependent spinodals, the structure of steady states depends significantly on pre-existing structures (memory effect). For a homogeneous initial alloy with slight initial noise, decomposition is suppressed everywhere beyond the rate-dependent spinodal. If the initial structure is prepared by shifting composition or temperature into an instability region and then returning it beyond the spinodal after partial decomposition, the alloy’s behavior varies. Closer to the spinodal (but still beyond it), the steady state tends toward a cheetah-type (gепard-like) decomposition; in

the remaining area between the spinodal and binodal, the alloy stays uniform.

6. Our system shows both compositional and temperature hysteresis: by using a previous structure as the initial condition for a new simulation with an altered deposition composition or temperature, we demonstrate that steady states in alloys with the same composition, but different initial conditions, can lead to markedly different morphologies.

7. We derived a generalized evolution criterion (Eq. (23)) for the free energy of our open system.

8. We also studied the properties of an even more simplified model – when both exchanges and interaction energies are taken into account only within a single top plane. The results practically coincide with the main model after rescaling the temperature twice.

9. Ordering of patterns is found: In both models, the distribution of reduced cluster sizes as well as distribution of distances between nearest neighbors shows a tendency to become more and more narrow with increasing rate and temperature.

10. We also used the Monte Carlo version of the simplified model. The results are qualitatively similar. A detailed analysis of the influence of noise on hysteresis and memory (both thermal noise of atomic jump frequencies and noise from the deposition flux) will be published elsewhere.

11. The mean-field version of our model seems more preferable for further investigation of the fundamental physics of open systems, including kinetic equations for transitions between different steady states due to changes in temperature, deposition rate, or the initial structure.

Authors are grateful for the “ENSEMBLE3-Center of Excellence for Nanophononics, Advanced Materials and Novel Crystal Growth-Based Technologies” project (GA No. MAB/2020/14), carried out under the International Research Agenda programs of the Foundation for Polish Science that are co-financed by the European Union under the European Regional Development Fund and the European Union Horizon 2020 Research and Innovation Program Teaming for Excellence (GA No. 857543) for supporting this work. The publication was created as a part of the project of the Minister of Science and Higher Education “Support for the Activities of Centers of Excellence Established in Poland under the Horizon 2020 Program” under contract

No. MEiN/2023/DIR/3797. Authors are also grateful to Prof. King Ning Tu, to Dr. Ihor Radchenko and to Anastasiia Titova for fruitful discussions of phase and structural transitions in open systems.

APPENDIX A.

Absolute Instability Criterion for Closed System ($v = 0$)

According to Eqs. (9) and (10), we are looking for a solution in the form of a concentration wave with infinitesimal amplitude A for two planes of the FCC lattice:

$$C_A(i, j, k = 0) = C^{\text{dep}} + A \exp \left[I \frac{a}{2} (q_x i + q_y j) \right], \quad i + j = 2m, \quad (\text{A1})$$

$$C_A(i', j', k' = 1) = C^{\text{dep}} + A \exp \left[I \frac{a}{2} (q_x i' + q_y j') \right] \times \frac{1}{2} \left(\cos \left(\frac{q_x a}{2} \right) + \cos \left(\frac{q_y a}{2} \right) \right), \quad i' + j' = 2m + 1. \quad (\text{A2})$$

We substitute Eqs. (A1) and (A2) into Eq. (8), expanding everything into a series over small A and neglecting the second-order and higher-order terms. For example,

$$\exp \left[\frac{E_{\text{mix}}}{kT} \left(\sum_{in'=1}^Z \delta C(in') - \sum_{i'=1}^Z \delta C(i') \right) \right] \approx \approx 1 + \frac{E_{\text{mix}}}{kT} \left(\sum_{in'=1}^Z \delta C(in') - \sum_{i'=1}^Z \delta C(i') \right).$$

We get

$$\begin{aligned} \frac{\partial \delta C(i)}{\partial t t} &= -Z_{\parallel} \delta C(i) + \\ &+ \sum_{in=1}^{Z_{\parallel}} \delta C(in) - \frac{2E_{\text{mix}}}{kT} C^{\text{dep}} (1 - C^{\text{dep}}) \times \\ &\times \left(\sum_{in'=1}^Z \delta C(in') - \sum_{i'=1}^Z \delta C(i') \right). \end{aligned} \quad (\text{A3})$$

We multiply both parts by $\frac{1}{A} \exp[-I \mathbf{q} \cdot \mathbf{r}_i]$. Then

$$\begin{aligned} \frac{\partial \ln A}{\partial t^2} &= \sum_{in=1}^{Z_{\parallel}} \exp \left[I \mathbf{q} \cdot (\mathbf{r}_{in} - \mathbf{r}_i) \right] - Z_{\parallel} - \\ &- \frac{2E_{\text{mix}}}{kT} C^{\text{dep}} (1 - C^{\text{dep}}) \times \\ &\times \sum_{in=1}^{Z_{\parallel}} \left\{ \sum_{in'=1}^{Z_{\parallel}} \exp \left[I \mathbf{q} \cdot ((\mathbf{r}_{in'} - \mathbf{r}_{in}) + (\mathbf{r}_{in} - \mathbf{r}_i)) \right] + \right. \\ &+ \sum_{in'=1}^{Z_{\perp}} \delta C(in') \frac{1}{A} \exp \left[-I \mathbf{q} \cdot \mathbf{r}_{in} \right] \times \\ &\times \exp \left[I \mathbf{q} \cdot (\mathbf{r}_{in} - \mathbf{r}_i) \right] - \sum_{i'=1}^{Z_{\parallel}} \exp \left[I \mathbf{q} \cdot (\mathbf{r}_{i'} - \mathbf{r}_i) \right] - \\ &\left. - \sum_{i'=1}^{Z_{\perp}} \delta C(i') \frac{1}{A} \exp \left[-I \mathbf{q} \cdot \mathbf{r}_i \right] \right\}. \end{aligned} \quad (\text{A4})$$

We naturally come to two kinds of structural factors related to different sums – (1) over nearest neighbors within plane $k = 0$ $(\frac{a}{2}, \frac{a}{2}), (\frac{a}{2}, -\frac{a}{2}), (-\frac{a}{2}, \frac{a}{2}), (-\frac{a}{2}, -\frac{a}{2})$, and (2) over nearest neighbors belonging to down plane $k = 1$ $(\frac{a}{2}, 0), (-\frac{a}{2}, 0), (0, \frac{a}{2}), (0, -\frac{a}{2})$:

$$\begin{aligned} S_1(\mathbf{q}) &= \sum_{in=1}^{Z_{\parallel}=4} \exp \left[I \mathbf{q} \cdot (\mathbf{r}_{in} - \mathbf{r}_i) \right] = \\ &= \exp \left[I \left(q_x \frac{a}{2} + q_y \frac{a}{2} \right) \right] + \exp \left[I \left(q_x \frac{a}{2} - q_y \frac{a}{2} \right) \right] + \\ &+ \exp \left[I \left(-q_x \frac{a}{2} + q_y \frac{a}{2} \right) \right] + \exp \left[I \left(-q_x \frac{a}{2} - q_y \frac{a}{2} \right) \right] = \\ &= 2 \left\{ \cos \left((q_x + q_y) \frac{a}{2} \right) + \cos \left((q_x - q_y) \frac{a}{2} \right) \right\} = \\ &= 4 \cos \left(q_x \frac{a}{2} \right) \cos \left(q_y \frac{a}{2} \right), \end{aligned} \quad (\text{A5})$$

$$\begin{aligned} S_2(\mathbf{q}) &= \sum_{in'=1}^{Z_{\perp}=4} \delta C(i') \frac{1}{A} \exp \left[-I \mathbf{q} \cdot \mathbf{r}_i \right] = \\ &= \left\{ \exp \left[I q_x \frac{a}{2} \right] + \exp \left[-I q_x \frac{a}{2} \right] + \right. \\ &+ \exp \left[I q_y \frac{a}{2} \right] + \exp \left[-I q_y \frac{a}{2} \right] \left. \right\} \times \\ &\times \frac{1}{2} \left[\cos \left(\frac{a}{2} q_x \right) + \cos \left(\frac{a}{2} q_y \right) \right] = \\ &= \left[\cos \left(q_x \frac{a}{2} \right) + \cos \left(q_y \frac{a}{2} \right) \right]^2. \end{aligned} \quad (\text{A6})$$

In these terms, Eq. (A4) transforms into:

$$\begin{aligned} \frac{\partial \ln A}{\partial t t} &= (S_1 - 4) \times \\ &\times \left\{ 1 - \frac{2E_{\text{mix}}}{kT} C^{\text{dep}} (1 - C^{\text{dep}}) (S_1 + S_2) \right\} = \\ &= 4 \left[1 - \cos \left(q_x \frac{a}{2} \right) \cos \left(q_y \frac{a}{2} \right) \right] \times \\ &\times \left\{ \frac{8E_{\text{mix}}}{kT} C^{\text{dep}} (1 - C^{\text{dep}}) \times \right. \\ &\times \left[\cos \left(q_x \frac{a}{2} \right) \cos \left(q_y \frac{a}{2} \right) + \right. \\ &\left. \left. + \frac{1}{4} \left(\cos \left(q_x \frac{a}{2} \right) + \cos \left(q_y \frac{a}{2} \right) \right)^2 \right] - 1 \right\}. \end{aligned}$$

APPENDIX B. Critical Velocity

$$\begin{aligned} v^{\text{critical}} &= \max_{(q_x, q_y)} \left\{ 4 \left[1 - \cos \left(q_x \frac{a}{2} \right) \cos \left(q_y \frac{a}{2} \right) \right] \times \right. \\ &\times \left[\frac{W}{2} \left(\cos \left(q_x \frac{a}{2} \right) \cos \left(q_y \frac{a}{2} \right) + \right. \right. \\ &\left. \left. + \left(\frac{\cos \left(q_x \frac{a}{2} \right) + \cos \left(q_y \frac{a}{2} \right)}{2} \right)^2 \right) - 1 \right] \right\}. \end{aligned} \quad (\text{B1})$$

Let $x = \cos(q_x \frac{a}{2})$ and $y = \cos(q_y \frac{a}{2})$,

$$v^{\text{critical}} = \max \Psi(x, y) = \max \left\{ 4 [1 - xy] \times \left[\frac{W}{2} \left(xy + \left(\frac{x+y}{2} \right)^2 \right) - 1 \right] \right\}. \quad (\text{B2})$$

The partial derivatives of Ψ with respect to x and y must be zero at the maximum. Therefore, the combination $x \frac{\partial \Psi}{\partial x} - y \frac{\partial \Psi}{\partial y} = 2W(x^2 - y^2) = 0$, indicating that the optimal concentration wave should be along the diagonal direction. Taking $x = y$ in Ψ , one may easily find the maximum condition and maximal value:

$$\Psi(x = y) = 4 [1 - x^2] [Wx^2 - 1] = \max \implies x_{\text{opt}}^2 = \frac{W+1}{2W},$$

$$v^{\text{critical}}(\langle 110 \rangle) = \Psi(x_{\text{opt}}) = \frac{(W-1)^2}{W}. \quad (27)$$

1. M. Henkel, H. Hinrichsen, S. Lübeck. *Non-Equilibrium Phase Transitions. Vol. 1. Absorbing Phase Transitions* (Springer, 2008).
2. G. Martin, P. Bellon. Radiation effects in concentrated alloys and compounds: equilibrium and kinetics of driven systems. *Comptes Rendus Physique* **9** (3–4), 323 (2008).
3. Y. Ashkenazy, N.Q. Vo, D. Schwen, R.S. Averback, P. Bellon. Shear induced chemical mixing in heterogeneous systems. *Acta Materialia* **60** (3), 984 (2012).
4. B.B. Straumal, A.S. Gornakova, O.B. Fabrichnaya, M.J. Kriegel, A.A. Mazilkin, B. Baretzky, S.V. Dobatkin. Effective temperature of high pressure torsion in Zr–Nb alloys. *High Temperature Materials and Processes* **31** (4–5), 339 (2012).
5. S.G. Brush. History of the Lenz–Ising model. *Rev. Mod. Phys.* **39** (4), 883 (1967).
6. G. Martin. Atomic mobility in Cahn–Hilliard diffusion model. *Phys. Rev. B* **41** (4), 2279 (1990).
7. Z. Erdélyi, I.A. Szabó, D.L. Beke. Interface sharpening instead of broadening by diffusion in ideal binary alloys. *Phys. Rev. Lett.* **89** (16), 165901 (2002).
8. D.L. Beke, Z. Erdélyi. Resolution of the diffusional paradox predicting infinitely fast kinetics on the nanoscale. *Phys. Rev. B* **73** (3), 035426 (2006).
9. Z. Erdélyi, M. Pasichnyy, V. Bezpalchuk, J.J. Tomán, B. Gajdics, A.M. Gusak. Stochastic kinetic mean field model. *Computer Phys. Commun.* **204**, 31 (2016).
10. T.V. Zaporozhets, A. Taranovskyy, G. Jáger, A.M. Gusak, Z. Erdélyi, J.J. Tomán. The effect of introducing stochasticity to kinetic mean-field calculations: Comparison with lattice kinetic Monte-Carlo in case of regular solid solutions. *Comput. Mater. Sci.* **171**, 109251 (2020).
11. B. Gajdics, J.J. Tomán, H. Zapolsky, Z. Erdélyi, G. Demange. A multiscale procedure based on the stochastic kinetic mean field and the phase-field models for coarsening. *J. Appl. Phys.* **126** (6), 065106 (2019).
12. A. Gusak, T. Zaporozhets, N. Storozhuk. Phase competition in solid-state reactive diffusion revisited – Stochastic kinetic mean-field approach. *J. Chem. Phys.* **150** (17), 174109 (2019).
13. A. Titova, H. Zapolsky, A. Gusak. Memory effects during co-deposition of binary alloys. *Scripta Materialia* **241**, 115897 (2024).
14. Y. Lu, B. Derby, H. Sriram, K. Kadirvel, C. Wang, X. Liu, Y. Wang. Microstructure development and morphological transition during deposition of immiscible alloy films. *Acta Materialia* **220**, 117313 (2021).
15. M. Powers, J.A. Stewart, R. Dingreville, B.K. Derby, A. Misra. Compositionally-driven formation mechanism of hierarchical morphologies in co-deposited immiscible alloy thin films. *Nanomaterials* **11** (10), 2635 (2021).
16. S. Akamatsu, S. Bottin-Rousseau, M. Şerefoğlu, V.T. Witusiewicz, U. Hecht, M. Plapp. In situ experiments in microgravity and phase-field simulations of the lamellar-to-rod transition during eutectic growth. *Comptes Rendus. Mécanique* **351** (S2), 1 (2023).
17. S. Bottin-Rousseau, V.T. Witusiewicz, U. Hecht, J. Fernandez, A. Laveron-Simavilla, S. Akamatsu. Coexistence of rod-like and lamellar eutectic growth patterns. *Scripta Materialia* **207**, 114314 (2022).
18. M. Şerefoğlu, S. Bottin-Rousseau, S. Akamatsu. Lamellar-rod pattern transition and confinement effects during eutectic growth. *Acta Materialia* **242**, 118425 (2023).
19. L. Rátkai, G.I. Tóth, L. Környei, T. Pusztai, L. Gránásy. Phase-field modeling of eutectic structures on the nanoscale: The effect of anisotropy. *J. Mater. Sci.* **52**, 5544 (2017).
20. A. Gusak, A. Titova. Eutectic crystallization and melting in sharp concentration gradients. *J. Chem. Phys.* **158** (16), (2023).
21. M. Atzmon, D.A. Kessler, D.J. Srolovitz. Phase separation during film growth. *J. Appl. Phys.* **72** (2), 442 (1992).
22. J.W. Cahn, J.E. Hilliard. Free energy of a nonuniform system. I. Interfacial free energy. *J. Chem. Phys.* **28** (2), 258 (1958).
23. A.A. Vlasov. *Theory of Many Particles* (Gostekhizdat, 1950).
24. A.G. Khachatryan. *Theory of Structural Transformations in Solids* (Courier Corporation, 2013).
25. A.S. Shirinyan, A.M. Gusak. Phase diagrams of decomposing nanoalloys. *Philosophical Magazine* **84** (6), 579 (2004).
26. A.S. Shirinyan, A.M. Gusak, M. Wautelet. Phase diagram versus diagram of solubility: What is the difference for nanosystems? *Acta Mater.* **53** (19), 5025 (2005).
27. A.M. Gusak, A.O. Kovalchuk, B.B. Straumal. Interrelation of depletion and segregation in decomposition of nanoparticles. *Philosophical Magazine* **93** (14), 1677 (2013).

Received 27.05.25

A.M. Gusak, S.O. Abakumov

СПРОЩЕНА КІНЕТИЧНА МОДЕЛЬ
ФАЗОВИХ ПЕРЕХОДІВ І КОНКУРЕНЦІЇ
СТРУКТУР У ВІДКРИТІЙ ДВОВИМІРНІЙ СИСТЕМІ

Апроксимація регулярного розчину успішно застосовується в термодинаміці та кінетиці розкладання сплавів, де вони розглядаються як замкнуті системи. Ця апроксимація забезпечує якісно правильний опис усіх стадій як спінодального, так і опосередкованого стадією зародження розпадів сплавів за однорідних зовнішніх умов та без зовнішніх потоків. У цій статті кінетичну модель середнього поля для відкритих (керованих потоком) систем розширено шляхом включення розбіжності вхідних і вихідних потоків у основні рівняння для ймовірностей заселення. Найближчим експериментальним аналогом цієї моделі є формування структури під час спільного осадження бінарного сплаву в умовах замороженої об'ємної дифузії, але з прийнятною поверхне-

вою дифузією, де швидкість осадження V є основним зовнішнім параметром. Однак деякі особливості моделі також можуть бути корисними для опису евтектичної та позаевтектичної кристалізації. Для стаціонарних станів такої відкритої системи визначені залежні від швидкості V фазові діаграми температура–концентрація. Область нестабільності, що залежить від V , підрозділяється на три різні стаціонарні морфології: “гепардоподібні” плями, “зеброподібні” смуги (ламелярні та лабіринтові структури), та їх комбінації. Ця морфологічна карта залежить від початкових умов, проявляючи ефекти пам'яті та гістерезис. Це означає, що на відміну від стану рівноваги у замкнутій системі, яка діє як аттрактор для шляхів еволюції, стаціонарні стани керованих потоком систем можуть не бути аттракторами.

Ключові слова: відкрита система, керовані потоками фазові переходи, спінодальний розклад, формування структури, залежна від швидкості фазова діаграма, гістерезис.